Functional Allocation of Synaptic Contacts in Microcircuits From Rods Via Rod Bipolar to AII Amacrine Cells in the Mouse Retina

Yoshihiko Tsukamoto,[1,2]* and Naoko Omi[1]

[1]Studio Retina, Satonaka, Nishinomiya, Hyogo 663-8183, Japan
[2]Department of Biology, Hyogo College of Medicine, Nishinomiya, Hyogo 663-8501, Japan

ABSTRACT

Retinal microcircuits for night vision at the absolute threshold are required to relay a single-photon rod signal reliably to ganglion cells via rod bipolar (RB) cells and AII amacrine cells. To assess the noise reduction of intercellular signal transmission in this rod-specific pathway, we quantified its synaptic connectivity by 3D reconstruction of a series of electron micrographs. In most cases (94%), each rod made ribbon synaptic contacts onto two adjacent RB cells. Conversely, each RB cell was contacted by 25 rods. Each RB axon terminal contacted four or five AII amacrine cells via 53 ribbon synapses. Thus, the signal from one rod may be represented as 106 replicates at two RB axons. Moreover, the two adjacent RB cells contacted two to four AII amacrine cells in common, where the signals relayed by two RB cells were reunited. In more detail, over 50% of each RB output was directed predominantly to a single, preferred AII amacrine cell, although each RB cell also separately contacted another one to three AII amacrine cells. Most of the replicate signals at two RB axons were collected on a few AII amacrine cells via reunions, dominant connections, and electrical coupling by AII–AII gap junctions. Thus the original signal may be reliably represented by signal amplification with focal accumulation without gathering unnecessary noise from a wide surrounding area. This allocation of RB–AII synaptic contacts may serve as the structural basis for the physiological properties of the AII single-photon response that include high amplification, local adaptation, and regenerative acceleration. J. Comp. Neurol. 521:3541-3555, 2013.

INDEXING TERMS: ribbon synapse; neural connection; photon signal; noise reduction; electron microscopy; scotopic vision

At low scotopic background levels, a single-photon signal in a rod is reliably relayed by rod bipolar (RB) and AII amacrine to ganglion cells amidst neural noise (Barlow et al., 1971; Baylor et al., 1979, 1984; Mastronarde, 1983; Rieke, 2008). A key mystery at the first stage of this pathway was clarified when noise removal from scotopic rod signals by a thresholding nonlinearity at the rod–RB synapse was demonstrated computationally (van Rossum and Smith, 1998) and experimentally (Field and Rieke, 2002; Sampath and Rieke, 2004). However, the 3D microcircuit architecture by which single-photon signals are transmitted through the next stage of this rod-specific relay pathway is unclear.

Physiological studies on mouse retinas have clarified several characteristics of the RB–AII synapse, such as a thresholding mechanism with multivesicular release (Singer et al., 2004), high amplification (Pang et al., 2004, 2007), and adaptation to avoid saturation and to code contrast (Dunn et al., 2006; Dunn and Rieke, 2008; Oesch and Diamond, 2011). AII–AII electrical synapses synchronously promote bidirectional transmission of subthreshold potentials and sodium channel spikes (Veruki and Hartveit, 2002). For efficient signal-to-noise ratio (S/N) improvement in rod-driven signals during this electrical coupling, it was hypothesized that the anatomical divergence of the signal from one rod

Grant sponsor: Japan Society for the Promotion of Science Grant-in-Aid for Scientific Research; grant number: 22500317 (to Y.T.).

*CORRESPONDENCE TO: Yoshihiko Tsukamoto, PhD, Studio Retina, 2-7-6, Satonaka, Nishinomiya, Hyogo 663-8183, Japan. E-mail: ytsuka@hyo-med.ac.jp

Received December 24, 2012; Revised May 7, 2013;
Accepted for publication May 23, 2013.
DOI 10.1002/cne.23370
Published online June 8, 2013 in Wiley Online Library (wileyonlinelibrary.com)

through RB cells onto AII amacrine cells and the space constant of AII–AII electrical coupling should coincide (Smith and Vardi, 1995). The electrical coupling producing this particular space constant will reduce uncorrelated synaptic noise while collecting the divergent rod signal without much decrement. The receptive field of an AII amacrine cell in dark-adapted rabbit retinas is 60–80 μm across, which is much smaller than the receptive field of approximately 400 μm measured in the mesopic range (Bloomfield et al., 1997; Bloomfield and Xin, 2000; Bloomfield, 2001). These measurements, showing that the receptive field of an AII amacrine cell at low scotopic levels is limited, support the hypothesis that the RB–AII synapse at low scotopic levels is involved in selectively transmitting the single-photon response from a rod with high gain through the two RB cells it contacts, without collecting much synaptic noise from neighboring RB cells (Smith and Vardi, 1995). However, the circuit divergence of one rod signal via RB to AII amacrine cells has not been clarified precisely by observation of all contacts along its pathways.

This study examines how a single-photon signal could be conveyed to AII amacrine cells. To elucidate the structural constraints for stage-by-stage signal transmission in the central area of the mouse retina, we identified every synaptic contact along each pathway of the signal derived from a rod. We reconstructed a map of rod photoreceptor–RB synapse and a map of synaptic convergence from RB terminals to AII amacrine cells and counted nearly all chemical and electrical synapses of three AII amacrine cells. Thus, we determined the synaptic connectivity of the RB–AII pathway and analyzed it from the viewpoint of information processing.

MATERIALS AND METHODS

Preparations

For 3D reconstruction of retinal neurons in this study, we used the same series of electron micrographs of the central retina of the mouse (C57BL/6J, female, 20 g, 9 weeks old; provided by Japan SLC, Shizuoka, Japan) used in our previous study (Tsukamoto et al., 2001). In brief, the mouse was deeply anesthetized with sodium pentobarbital (45 mg/kg i.p.) and perfused with a fixative containing 2% paraformaldehyde, 2.5% glutaraldehyde, and 1% acrolein in phosphate buffer (0.1 M, pH 7.4). The right eyeball was enucleated, and the posterior pole of the retina was immersed in the same fixative, with 1% tannic acid replacing the acrolein. The tissue was postfixed with 1% osmium tetroxide for 2 hours, stained with 3% uranyl acetate in 80% methanol, dehydrated with ethanol, and embedded in araldite resin. This procedure was performed in compliance with the *Guide for the care and use of experimental animals* of Hyogo College of Medicine.

Electron micrographs

A series of 366 radial sections was cut at a thickness of 90 nm. Sections were mounted on formvar-covered single-slot grids, stained with uranyl acetate and lead citrate, and photographed at ×3,000 using JEM1200EX and JEM1220 electron microscopes (JEOL, Tokyo, Japan) at the Joint-Use Research Facilities, Hyogo College of Medicine. Certain synapses were rephotographed at ×40,000 with various tilts. Digital images of electron micrographs were captured by a GT-X970 digitizer (Epson, Nagano, Japan), followed by software manipulation of brightness and contrast (Photoshop in Adobe CS2; Adobe Systems, San Jose, CA). Illustrator in Adobe CS2 was also used for graphic representations. Three-dimensional images were reconstructed using TRI/3D-SRF-R graphic software (Ratoc Systems International, Tokyo, Japan) for Windows XP.

Measurements

The cell-level analysis of neural connectivity clarifies convergence and divergence. Convergence (or divergence) is the number of presynaptic (or postsynaptic) cells that have at least one contact with a specific postsynaptic (or presynaptic) cell. However, it does not necessarily determine the number of synaptic contacts for each cell-to-cell connection. Here we carried out the contact-level analysis to determine the number of synaptic contacts for each cell-to-cell connection involved in its specific convergence and divergence. We characterized the connections from pre- to postsynaptic cells at rod–RB and RB–AII amacrine interfaces by counting individual contacts on electron micrographs. The data in the text are presented as the mean ± SD.

RESULTS

Reconstruction of AII amacrine cells

We reconstructed the 3D morphology of three adjacent AII amacrine cells (AII 1, 2, and 3) and almost all their input and output synapses, as shown in Figure 1. Their dendrites exhibited the following four morphological traits: 1) a few short dendrites protruding from the soma around the border between the inner nuclear layer (INL) and inner plexiform layer (IPL), 2) several lobular dendrites extending horizontally from the descending shaft in sublamina a (strata 1 and 2) of the IPL, 3) a terminal dendritic arborization (or distal dendrites) arranged as a conical tuft comprising processes extending across sublamina b (strata 3, 4, and 5) of the IPL toward the ganglion cell layer, and 4) an axon initial

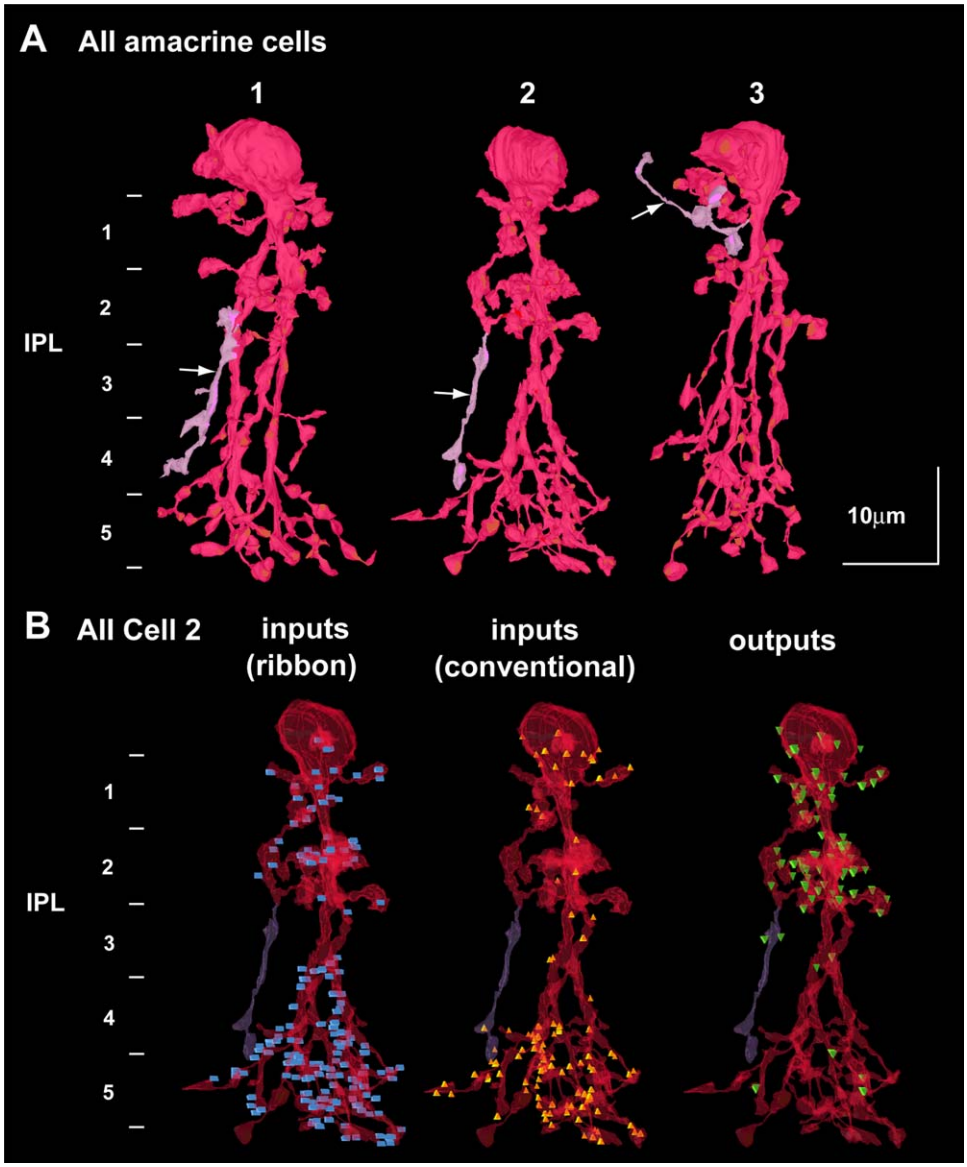

Figure 1. Mouse AII amacrine cells used for analysis. **A:** Three almost completely reconstructed AII amacrine cells (1, 2, and 3). Arrows indicate AIS-like dendrites. **B:** The distribution of chemical synapses in cell 2; the inputs in blue are the postsynaptic sites of the ribbon synapses, the inputs in orange are the postsynaptic sites of the conventional synapses, and the outputs in green are the presynaptic sites of the conventional synapses. Scale bars = 10 μm.

segment (AIS)-like dendritic process extending downward to terminate in stratum 4 (AII 1 and 2) or obliquely upward to terminate in the INL (AII 3). Recently, Wu et al. (2011) revealed the AIS-like process of an AII amacrine cell by expressing channel rhodopsin-2 (ChR2)-green fluorescent protein (GFP) with the AIS-targeting motif of Na_vII–III. They also stained the AIS-like processes by their immunoreactivity with ankyrin-G. According to their morphological characterization of the orientation, conformation, and termination of the AIS-like processes, we identified the AIS-like processes in our reconstructed AII amacrine cells in a different color (pink vs. red) in Figure 1. The branching point of the AIS-like process of every AII amacrine cell was located in sublamina a.

The AII amacrine cells received input at ribbon synapses from RB cells in sublamina b and from Off bipolar cells in sublamina a (Fig. 1B, blue rectangles; mean ± SD, 173 ± 7.5 sites, n = 3). We also observed conventional synapses whose presynaptic sites were characterized by a thick membrane, dense granular material, and clustered vesicles over the entire IPL (Fig. 1B, orange triangles; 98.3 ± 18.8 sites, n = 3). These were considered to be chemical synapses from other amacrine cells to AII amacrine cells. Output synapses were distributed primarily in sublamina a (Fig. 1B, green triangles; 91.7 ± 15.3 sites, n = 3), where

they were largely directed at Off bipolar cells. Pang et al. (2012) recently classified AII amacrine cells into three subtypes in the mouse retina based on physiological properties of synaptic inputs; subtype 1 cells received inputs from both RB and M-cone bipolar cells, subtype 2 received inputs primarily from RB cells, and subtype 3 received inputs mainly from M-cone bipolar cells with minor RB inputs. AII 1, 2, and 3 analyzed in our study are thought to correspond to their subtype 1 based on the afore-mentioned morphological input characteristics.

In addition, we identified four more AII amacrine cells, although only their neuronal processes were traced. These novel reconstructions and identifications, which extended our previous studies (Tsukamoto et al., 2001, 2007; Ishii et al., 2009), are used to describe the neuronal connections in the following analysis.

Electron micrographs of synapses

In the OPL, a rod photoreceptor spherule contained two ribbon-associated synaptic active zones directed at two invaginating dendrites, in most cases, extending from the two nearest RB cells (Fig. 2A). Infrequently, we found within the spherule a Y-shaped RB invaginating dendrite (Boycott and Kolb, 1973; Linberg et al., 2001) with two

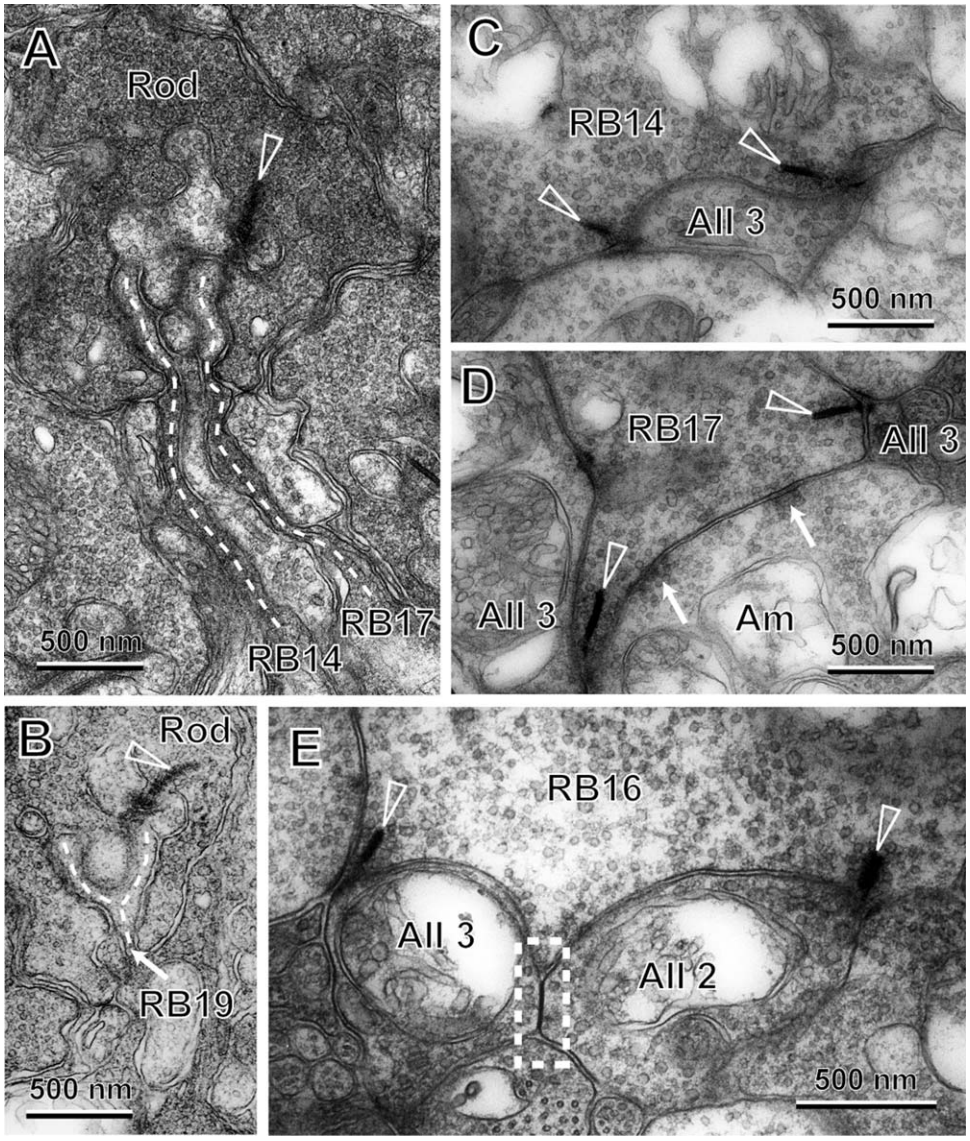

Figure 2. Electron micrographs at key points of the rod–RB–AII amacrine circuit. **A:** Divergence of a rod photoreceptor to two RB cells (RB14 and RB17) through the ribbon synapse (arrowhead) in its spherule. **B:** Y-shaped bifurcation of the RB-invaginating dendrite (RB19) within the rod spherule. **C,D:** Convergence of RB14 (C) and RB17 (D) to a common AII amacrine cell 3 through the ribbon synapses (arrowheads) at their axon terminals. Another type of amacrine cell makes conventional synapses (arrows) with RB17 in D. **E:** Gap junction (rectangle) between adjacent AII amacrine cells 2 and 3 is located close to the ribbon synapses (arrowheads) for their inputs from a common RB cell (RB16). Scale bars = 200 nm.

dendritic tips branching from a single proximal dendrite inside the spherule (Fig. 2B). We also rarely found two invaginating dendrites branching from a single proximal RB dendrite outside the spherule. In these two unusual cases, the rod output was considered to be directed at a single RB cell through two active zones. In the IPL, the two RB cells postsynaptic to a common rod photoreceptor were, in most cases, presynaptic to a common AII amacrine cell, as shown in Figure 2A,C,D (RB14 and RB17 → AII 3). This suggests that the signals from one rod that diverge onto two RB cells may reunite at the same AII amacrine cell. Furthermore, we frequently observed a gap junction between adjacent AII processes located close to the synaptic ribbons providing input to both AII amacrine cells from an individual RB cell, as shown in Figure 2E (RB16 → AII 2 and AII 3 connected by a gap junction).

Divergence and convergence from rod to RB cells and from RB to AII amacrine cells

AII 3 collected rod-driven signals from 174 rods through nine (eight completely and one incompletely reconstructed) RB cells, as shown in Figure 3. The

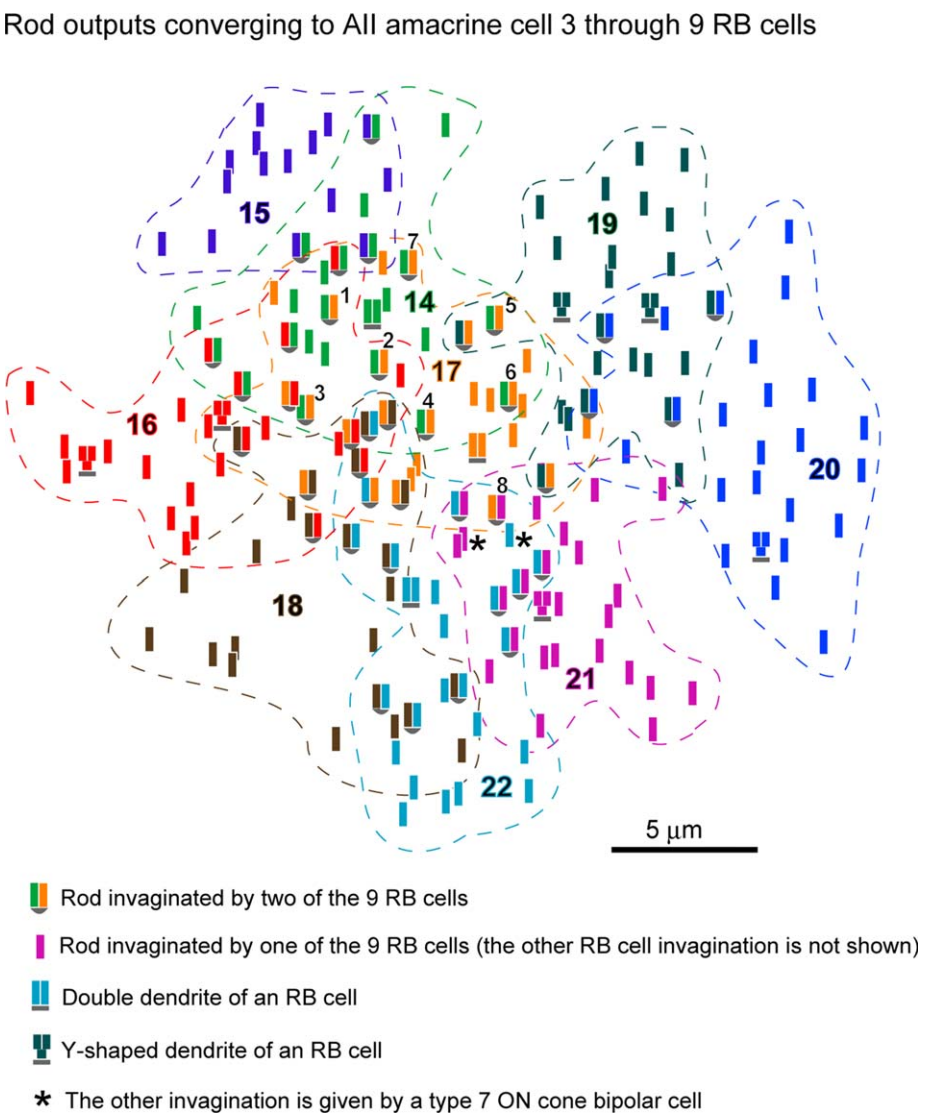

Figure 3. Map of RB synapses. A total of 174 rods synaptically converged to AII amacrine cell 3 through nine RB cells. The rods are shown divided into four groups: 1) 41 rods converging through a pair of Rbs, 2) 124 rods converging through one of the nine RB cells and one more RB cell outside the group of nine (not shown) or a type 7 On cone bipolar cell (asterisk), 3) three rods converging through the invaginating double dendrite of an RB cell (at RB14, 17, and 22), and 4) six rods converging through the Y-shaped RB invaginating dendrite (at RB16, 19, 20, and 21). The dotted contours in different colors indicate the dendritic fields of the nine RB cells (RB14–22). A bar of each color represents one of the RB invaginating dendrites. The number of rods converging onto each RB cell ranges from 24 to 27, with an average of 25, except for RB15 in the upper left, for which only 15 bars are shown because the others were not reconstructed (outside the series). Scale bar = 5 µm.

number of rods converging on each RB cell ranged from 24 to 27, with an average of 25 (25 ± 1, n = 8), except for RB15 in the upper left of Figure 3 (for which only 15 rods were identified because of the end of the series). Each of the 41 rods (23.6%) contacted a pair of invaginating dendrites of different RB cells among the nine RB cells connected to AII 3. Each of the 124 rods contacted one invaginating dendrite extending from one of the nine RB cells and with another invaginating dendrite (not shown in Fig. 3) extending from an RB cell outside these nine RB cells (122 rods, 70.1%) or a type 7 On cone bipolar cell (two rods, 1.1%; Tsukamoto et al, 2007). Three other rods (1.7%) contacted a pair of invaginating dendrites branching from a proximal RB dendrite outside the spherule, and each of the remaining six rods (3.4%) contacted a Y-shaped RB invaginating dendrite that bifurcated within the spherule. Thus, most of the rods (93.7%) diverged to two RB cells, but a small number (6.3%) of rods diverged to one RB cell, yielding an average divergence of 1.94.

Eighty-two dendrites invaginating 41 rod spherules were routed through nine RB cells toward AII 3. Each pair of dendrites could convey the common rod signal from a rod to AII 3. The numbers of rods that a pair of RB cells commonly invaginated are shown in Table 1. For instance, RB17 shared seven rods with RB14, three rods with RB16, and so on. Thus RB17 shared 16 rods with six other RB cells inside the group of RB cells connected to AII 3. One of the remaining 11 rods had the double dendrite of RB17. The other 10 rods were shared by RB17 and some RB cells outside this group. Let us take an outside cell RB8, which shared one rod with RB17 and five rods with RB15. In such a manner, all rods depicted by single bars in Figure 3 were shared by one of the inside RB cells and one of the outside RB cells.

The axon terminal of each RB cell had approximately 55 ribbon synapses (55.2 ± 4, n = 15). At the postsynaptic side of each ribbon synapse, there were two amacrine cell processes, one of which was an AII amacrine cell in 96% of the cases. Thus, the average number of synaptic contacts made by an RB cell to AII amacrine cells was 53. These output ribbon synapses were directed at three to five nearby AII amacrine cells, but the proportion of ribbon synapses varied among the AII amacrine cells. RB cells sent most of their synaptic outputs to their "preferred" AII amacrine cells. For example, RB17 and RB21 sent 34 (64%) and 31 (58%) synaptic contacts commonly to their preferred AII 3 (Fig. 4).

TABLE 1.
Number of Ribbon Contacts of RB Cells Paired With Adjacent RB Cells

RB cell number[1]	RB cell number[1]									
	14	15	16	17	18	19	20	21	22	Total
14		3	4	7	0	0	0	0	0	
15	3		0	0	0	0	0	0	0	
16	4	0		2	3	0	0	0	0	
17	7	0	2		3	2	0	1	1	
18	0	0	3	3		0	0	0	6	
19	0	0	0	2	0		4	0	0	
20	0	0	0	0	0	4		0	0	
21	0	0	0	1	0	0	0		5	
22	0	0	0	1	6	0	0	5		
Subtotal	14	3	9	16	12	6	4	6	12	82

[1]Nine RB cells, 14–22, that reach AII amacrine cell 3 at their axon terminals have 82 ribbon contacts in 41 pairs in rod spherules.

Dominant connections between RB and AII amacrine cells

When an RB cell provides more than 50% of its total contacts to a particular preferred AII amacrine cell, we regard this RB cell or this connection as being dominant (Fig. 5A). A list of the dominant connections found in this study is given in Table 2. Sixty-one percent of the total number of ribbon outputs was usually directed at only one preferred AII amacrine cell (60.9% ± 6.5%, n = 9). Conversely, 26% of the total ribbon inputs to an AII amacrine cell were provided by only the dominant RB cell (26.4% ± 2.3%, n = 6). Two dominant RB cells contacting their "preferred" postsynaptic cell by the largest number of their ribbon synapses provided 35 and 29 to AII 1, 35 and 33 to AII 2, and 34 and 31 to AII 3 (Table 2). The RB cells that provided the third highest number of ribbon synapses provided 17 to AII 1, 25 to AII 2, and 24 to AII 3, followed by RB cells that provided progressively fewer ribbon synapses (Fig. 5B). On average, two dominant RB cells provided approximately 53% (52.8% ± 3.2%, n = 3) of the total ribbon inputs to an AII amacrine cell, and three RB cells (the two dominant plus the one that provided the third highest number of ribbon synapses) provided 70% (70.5% ± 7.1%, n = 3) of them.

The distal dendritic arbors of three fully reconstructed AII amacrine cells (1–3) and those of four partially reconstructed surrounding AII amacrine cells (4–7) had input synapses from a total of 22 RB axon terminals, as shown in Figure 6A. AII 1 had 129 ribbon contacts from 12 RB cells, AII 2 had 129 contacts from 12 RB cells, and AII 3 had 116 contacts from nine RB cells. Thus, on average, an AII amacrine cell collected 125 ribbon contacts (125 ± 7.5, n = 3) from 11 convergent RB cells (11 ± 1.7, n = 3). From a different viewpoint, the average number of synaptic contacts made by one RB cell to one AII amacrine cell was 10.8 ± 11 (n = 12) for AII 1, 10.8 ± 12.8 (n = 12) for AII 2, and 12.9 ± 12.8 (n = 9) for AII 3. The relatively

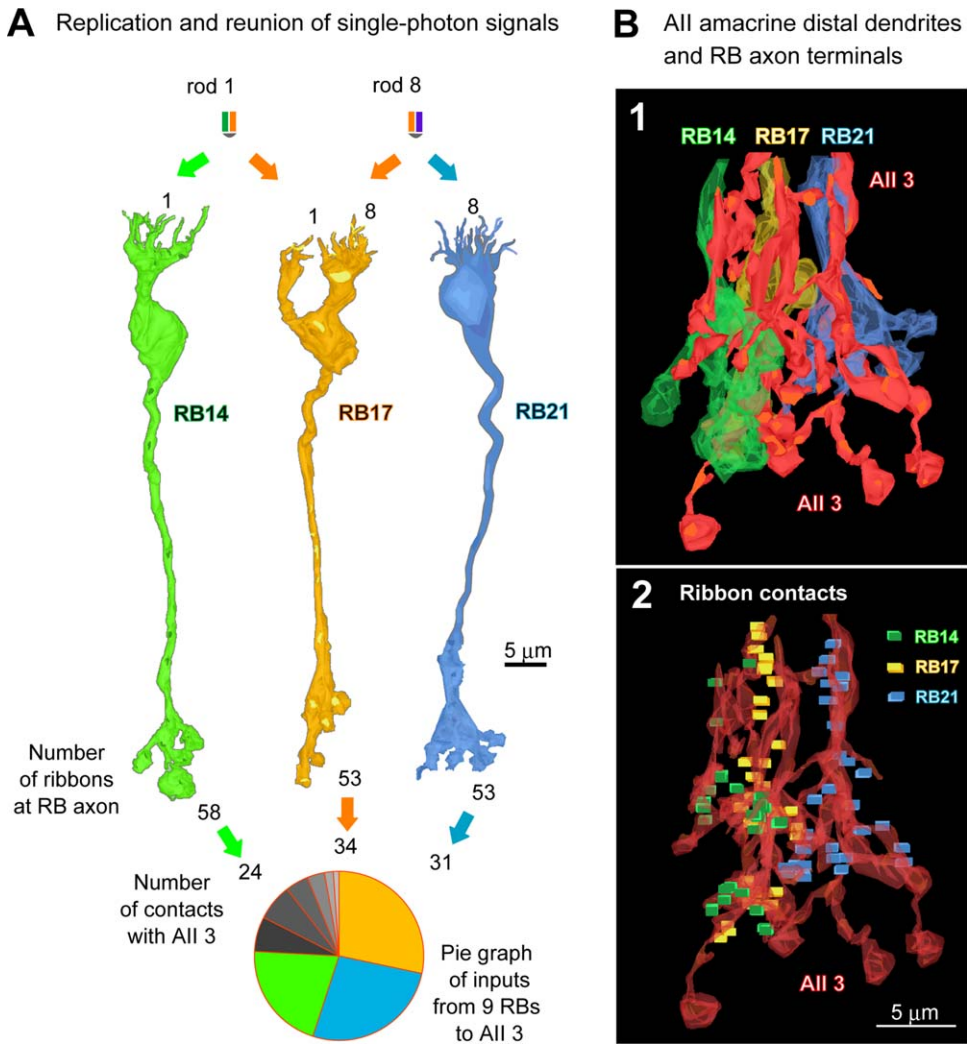

Figure 4. Pathway for bifurcation and reunion from single rods via pairs of RB cells to an AII amacrine cell 3. **A:** Rod 1 bifurcates to RB14 and RB17, and 24 of the 58 ribbon contacts at the RB14 axon and 34 of the 53 ribbon contacts at the RB17 axon are connected to AII 3. Likewise, the signals derived from rod 8 are reunited at AII 3 via 34 of the 53 contacts of RB17 and 31 of the 53 contacts of RB21. This AII amacrine cell receives a total of 116 inputs, 89 (77%) of which are provided by only these three major RB cells. Rods 1 and 8 correspond to the same rods as labeled in Figure 3. **B1:** The distal dendritic arbor (red) of AII 3 and the axon terminals of three major RB cells (RB14 in green, RB17 in yellow, and RB21 in blue). **B2:** Ribbon synapses in different colors, green for RB14, yellow for RB17, and blue for RB21. Scale bars = 5 µm.

large standard deviations indicated the large variability in the distribution of the number of synaptic contacts made by each RB cell directed to an AII amacrine cell. We determined the divergence from an RB cell to AII amacrine cells to be 4.7, using the relation that this value is equal to the ratio of the total number of contacts (53) made by an RB cell with all of its target AII amacrine cells to the average number of contacts (11.3 ± 11.9, n = 33) made by an RB cell to any one AII amacrine cell. We confirmed the validity of this measurement according to the equation (Freed et al., 1987; Sterling et al., 1988)

RB density/AII density = convergence/divergence

where the density of RB cells in this area was 24 × 10^3 cells/mm^2 and that of AII amacrine cells was 11 × 10^3 cells/mm^2, a density ratio of 2.2, which is fairly close to the convergence/divergence ratio of 2.3 (11/4.7). Because the density of rods in this area was 334 × 10^3 rods/mm^2, the density ratio of rods to RB cells was 14, and that of rods to AII amacrine cells was 30.

Reunion of rod-driven signals in AII amacrine cells

The convergence and divergence from 22 RB cells to seven AII amacrine cells are shown in Figure 6B. For

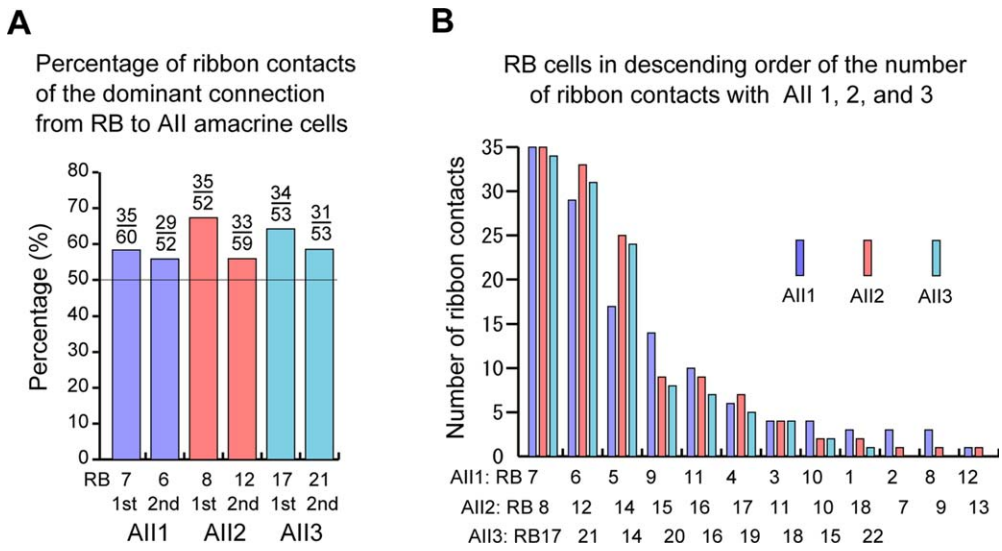

Figure 5. RB–AII connections. **A:** Dominant connections. The ratio of the number of contacts at the dominant connection to the total number of contacts for each RB cell is shown above each column. **B:** Histogram of ribbon contacts from RB cells to each AII amacrine cell (12 RB cells to AII 1, 12 RB cells to AII 2, and nine RB cells to AII 3). The abscissa shows the RB cells ordered by the number of contacts they make onto AII amacrine cells. The ordinate shows the number of ribbon contacts at each connection.

TABLE 2.

Ribbon Contacts for Dominant Connection From RB to AII Amacrine Cells

AII cell number[1]	RB cell number[1]	Dominant contacts	RB total contacts	% for RB (D/RB T)[2]	Two RB dominant contacts	AII total contacts	% for AII (2D/AII T)[3]
1	6	29	52	56	64	129	50
	7	35	60	58			
2	8	35	52	67	68	129	53
	12	33	59	56			
3	17	34	53	64	65	116	56
	21	31	53	58			
4	9	34	59	58	66	–	–
	11	32	57	56			
5	13	41	55	75	–	–	–
Mean		33.8	55.6	60.9	65.8	124.7	53.0
SD		3.3	3.2	6.5	1.7	7.5	3
n		9	9	9	4	3	3

[1]Specific combinations of RB cells and AII amacrine cells dominate (more than 50% of the total RB contacts) the number of synaptic contacts.
[2]Percentages of the dominant contacts for RB cells.
[3]Percentages of the dominant contacts for AII amacrine cells.

example, the nine RB cells (RB cells 14–22) converging onto AII 3 are labeled in light blue. Any pair of these nine RB cells could result in a reunited rod-driven signal at AII 3 if that pair of RB cells contacted any individual rod. In this case, 13 of the 36 possible pair combinations received reunited rod-driven signals. RB17 made reunion pairs with six nearby RB cells (14, 16, 18, 19, 21, and 22) but not with two distant RB cells (15 and 20; Table 1). RB15 made only one reunion pair with its neighbor, RB14, similar to RB20 with RB19. In particular, RB17 and RB21 provided 34 and 31 of the ribbon synapses, respectively, to their commonly preferred AII 3 (Figs. 5, 6B). Such dominant reunions were also found at AII 1 (29 from RB6 and 35 from RB7), AII 2 (35 from RB8 and 33 from RB12), and AII 4 (34 from RB9 and 32 from RB11).

Figure 6B also shows how many AII amacrine cells could be involved in the reunion of signals derived from one rod. For example, seven rods designated by numbers (1–7) in Figure 3 diverged to RB14 and RB17. These RB cells converged on AII 2 (pink) and AII 3 (blue). This suggests that the common rod-driven

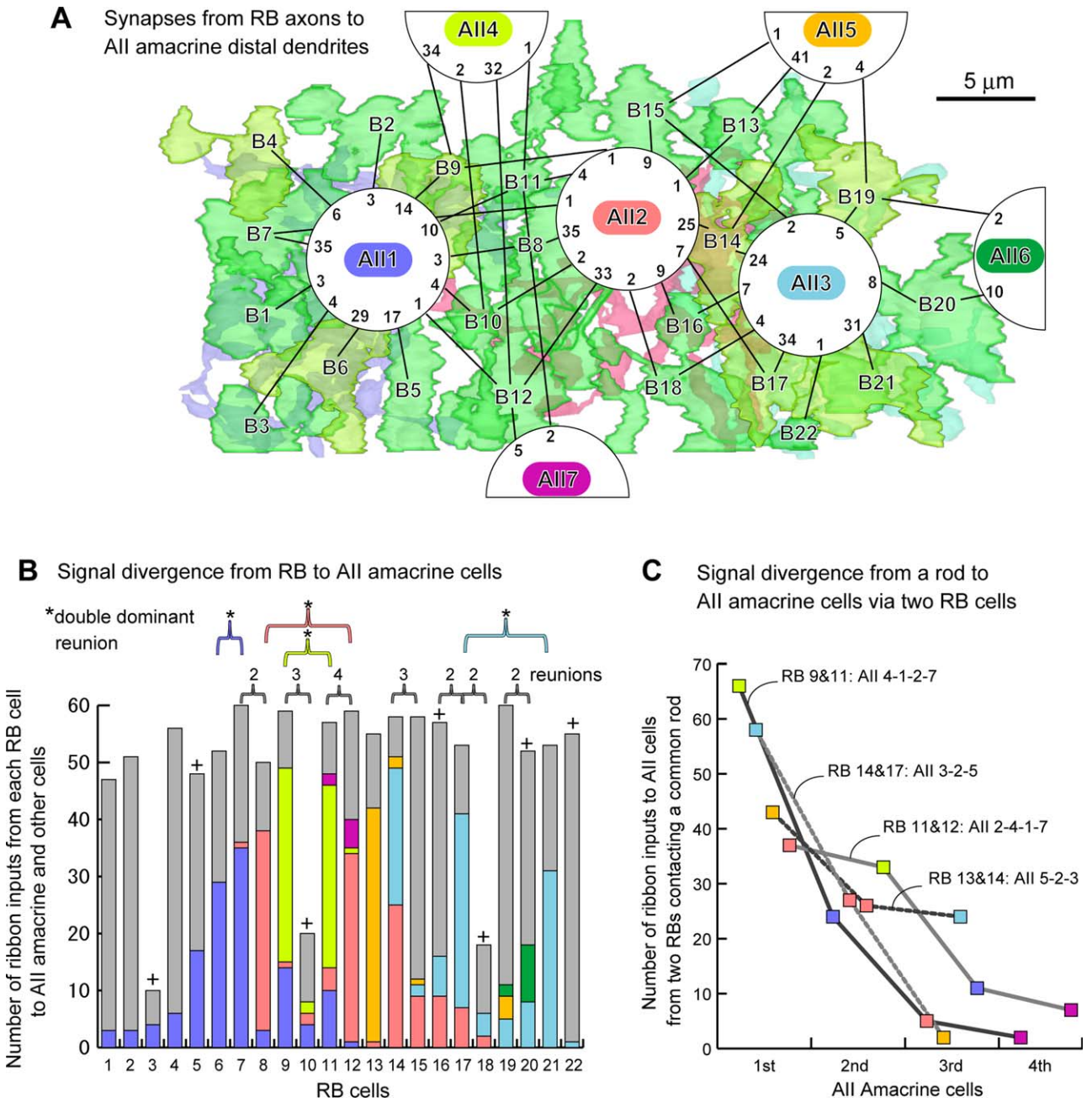

Figure 6. Ranking of synaptic contacts from RB to AII amacrine cells. **A:** The axon terminals of RB cells (B1–22) make ribbon synapses with the distal dendrites of AII amacrine cells (AII 1–7). The number of ribbon contacts for each RB–AII connection is shown at the periphery of a circle representing each AII amacrine cell. **B:** The cumulative numbers of ribbon contacts made by each RB cell (1–22) to AII amacrine cells (1–7 labeled in different colors, and unknowns in gray) are displayed in each column. The number of AII amacrine cells involved in reunions is shown by integers (2–4) above columns with brackets; e.g., common rod-driven signals of RB7 and RB8 may reunite at AII 3 (blue) and AII 2 (pink). Dominant reunion pairs of RB cells at a particular AII amacrine cell are found between RB6 and RB7 at AII 1 (blue, 64 contacts in total), RB8 and RB12 at AII 2 (pink, 68 contacts), RB17 and RB21 at AII 3 (light blue, 65 contacts), and RB9 and RB11 at AII 4 (green-yellow, 66 contacts). +, Partially reconstructed RB axon arbors. **C:** The number of RB ribbon contacts that could convey a common rod-driven signal to AII amacrine cells, each of which is designated by its corresponding color and plotted in descending order. The resulting weighting profile is sharpest for RB9 and RB11 (66, 24, five, and two contacts) but flattest for RB11 and RB12 (37, 33, 11, and seven contacts). Scale bar = 5 µm.

signals diverging to these two RB cells will reunite in two AII amacrine cells. By combining Table 1 and Figure 6B, we can further grasp that 22 rods (3, 4, 7, 2, 3, and 3 rods) are duplicated by six RB pairs (RB14–15, 14–16, 14–17, 16–17, 16–18, and 17–18, respectively) and reunited at both AII 2 and AII 3 cell. Reunions in

four AII amacrine cells were observed for the RB11 and RB12 pair located in fairly close proximity to AII 1 (blue), AII 2 (pink), AII 4 (green-yellow), and AII 7 (violet).

With the data described thus far, we can summarize the pathway of a single-photon rod signal as follows. A signal elicited by one rod is duplicated by two RB cells at their dendrites and multiplied at their axons by a factor of 53. One-hundred six common rod-driven signals are unevenly distributed to six or seven AII amacrine cells. Two to four of these AII amacrine cells reunite the common rod signals passing through two RB cells, but other AII amacrine cells receive those signals from only one of the two RB cells. For example, the signal elicited by one rod that diverged to RB9 and RB11 was routed to AII amacrine cells 4, 1, 2, 7, and one or two more (unknown cells shown in gray; Fig. 6B). The weighting profile tapered sharply (66, 24, five, and two contacts at AII amacrine cells 4, 1, 2, and 7, respectively; Fig. 6C), where AII amacrine cells 4, 1, and 2 were able to reunite the common signals derived from that rod but AII amacrine cell 7 was not. AII amacrine cell 4 was prominent because it received the common rod-driven signals via two dominant connections from RB9 (34 contacts: 58% of the total) and from RB11 (32 contacts: 56%). In contrast, AII amacrine cell 7 received those signals only from RB11 (two contacts: 4%). In one more case, the signal derived from a second rod that diverged to RB11 and RB12 was routed to AII amacrine cells 2, 4, 1, 7, and one or two more (Fig. 6B). The weighting profile tapered more moderately (37, 33, 11, and seven contacts at AII amacrine cells 2, 4, 1, and 7, respectively; Fig. 6C), where these four AII amacrine cells were able to reunite the common signals derived from the second rod. AII amacrine cell 2 received the common rod-driven signals via a weak connection from RB11 (four contacts: 7%) and a dominant connection from RB12 (33 contacts: 56%). In parallel, AII amacrine cell 7 received those signals via weak connections from both RB11 (2 contacts: 4%) and RB12 (five contacts: 9%). Thus the weighting profiles and the reunion patterns of the RB–AII connection carrying the common rod-driven signals varied depending on individual rods.

Gap junctions between AII amacrine cells

AII amacrine cells (1–3) were interconnected by gap junctions, which were distributed among their distal dendrites in sublamina b, as shown in Figure 7. Because the dendritic arbors of AII 1 and AII 3 did not overlap, they had no gap junctions, but they likely would communicate with each other through AII 2. These three AII amacrine cells were also interconnected by gap junctions to several surrounding AII amacrine cells (not shown). Because, in the cat retina, AII–AII gap junctions were found among AII proximal dendrites and somas in sublamina a as well as between AII distal dendrites in sublamina b (Vardi and Smith, 1996), we carefully examined sublamina a. However, we could not find any AII–AII gap junctions in sublamina a. The lack of gap junctions between the somas and soma-derived dendrites of AII amacrine cells was consistent with the wide AII–AII spacing relative to their dendritic arbors and the absence of any long, horizontal soma-derived dendrites in the mouse retina.

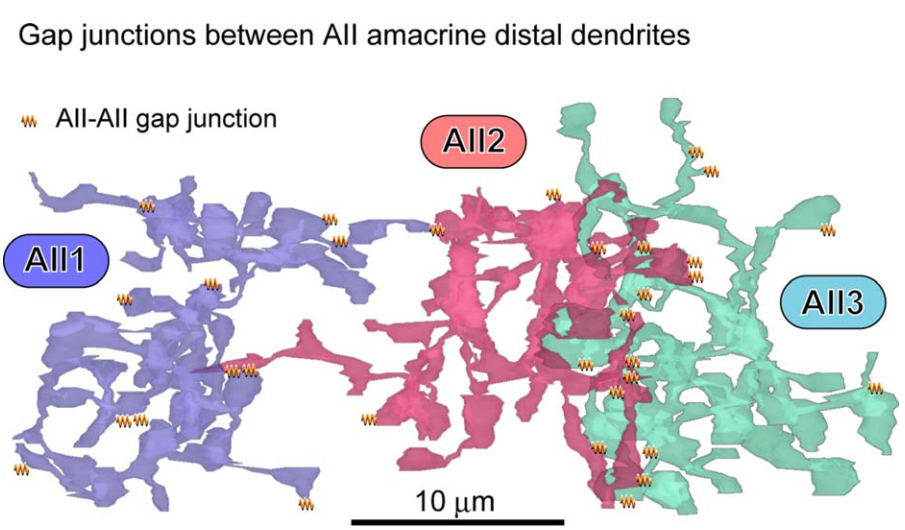

Figure 7. Allocation of AII–AII gap junctions. AII 1 has no gap junction with AII 3 because of their separation, but the intervening AII 2 has gap junctions with both AII 1 and AII 3. Every AII amacrine cell has gap junctions with other surrounding AII amacrine cells (not shown). Scale bar = 10 μm.

AIS-like process of an AII amacrine cell

In the context of regenerative amplification of rod-driven signals in AII amacrine cells (Veruki and Hartveit, 2002), it was important to examine whether their AIS-like dendritic processes (Fig. 1A) exhibited such ultrastructural features as found in the axon hillock and initial segment of typical neurons. The AIS of cortical neurons is characterized, among some other properties, by a dense layer of granular material that continuously undercoats the cell membrane (Palay et al., 1968; Peters et al., 1968). We observed many short and dense line segments attached to the cell membrane in the cytoplasm of the AIS-like processes of AII amacrine cell 3 (Fig. 8A,B). At higher magnification, they appeared to be tiny, dense layers of granular material discontinuously undercoating the cell membrane. Thus, in comparison with the AIS of cortical neurons, in which the cell membrane is typically completely undercoated, the cell membrane of the AII amacrine AIS-like processes was only intermittently undercoated (Fig. 8A,B). Nevertheless, the undercoating granular material appeared very similar in both cases. This unique feature was not detected in the ordinary, vitreally oriented dendrites of AII 3 (Fig. 8C). The AIS-like processes of AII 1 and 2 cells appeared to be mixed with both AIS-like and ordinary processes of AII 3 cell. The inputs and outputs at the AIS-like processes were as follows (Fig. 1A): RB ribbon inputs were connected to the AIS-like process of AII 1 cell via 14 contacts and to that of AII 2 via one contact, but there were no contacts with that of AII 3; conventional synaptic inputs were connected to AII 1 via five contacts, to that of AII 2 via two contacts, and to that of AII 3 via one contact; only two output synaptic contacts were found at that of AII 2 (green triangles at its proximal portion in Fig. 1B), but no contacts were found at that of AII 1 or AII 3. Furthermore, the AIS-like process of AII 1 or AII 2 cell had gap junctions with On bipolar cells in sublamina b, but that of AII 3 had none.

DISCUSSION

Our results clarify the nature of the microcircuits from each rod via RB cells to AII amacrine cells in the mouse retina, as illustrated in Figure 9. Most rods made ribbon contacts with two RB cells. Each RB cell established 53 ribbon synapses for RB–AII connections at the axon terminal. Two RB cells represented 106

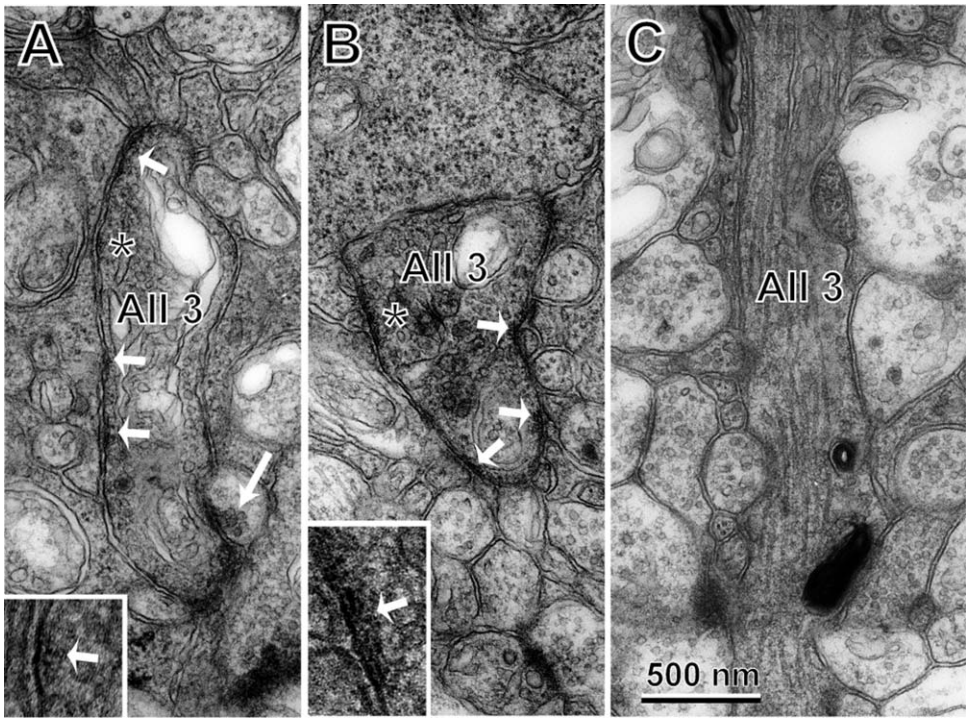

Figure 8. Electron micrographs of the AIS-like dendrites (A,B) and the ordinary dendrite (C) of AII amacrine cells. **A,B:** Many patches of dense material undercoating the surface membrane are observed (short arrows). An input synapse from the other amacrine cell is also seen (long arrow). **Insets:** High magnification of each labeled portion (asterisks). Patches of dark granular material appear just beneath the cell membrane (short arrows). **C:** The descending dendrite toward the distal arbor end of AII 3. No dense patches are observed. Scale bar = 500 nm.

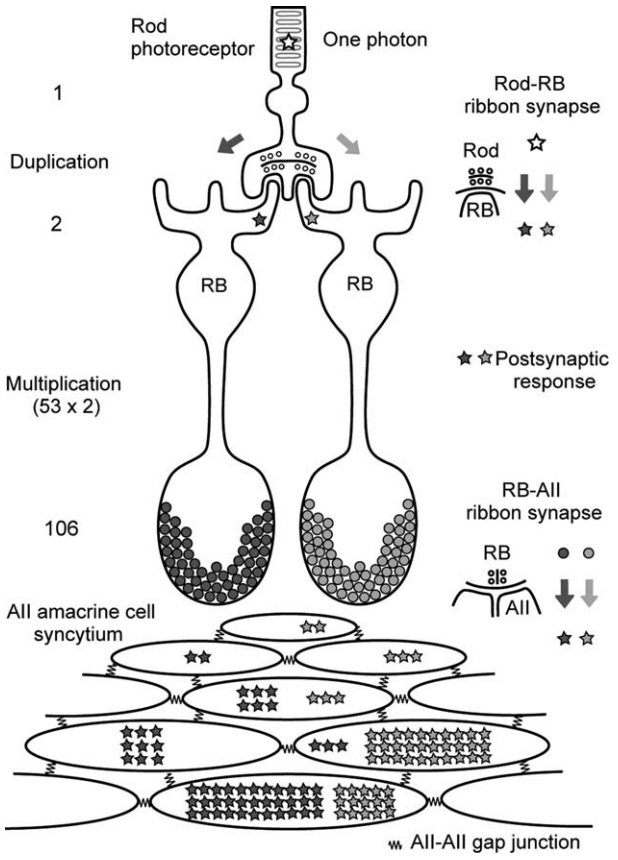

Figure 9. Diagram of the rod–RB–AII microcircuits in the mouse retina. Two RB cells make 106 replicates of a single-photon rod-driven signal at their axon terminals by duplication and multiplication. Most of the simultaneously replicated rod-driven signals are focused on a few AII amacrine cells via preferred pathways with signal reunions and without gathering unnecessary noise from a wide surrounding area.

copies of the original rod signal as synaptic contacts directed to six or seven AII amacrine cells. Two to four of those AII amacrine cells received contacts from these two RB cells, resulting in the reunion of the common rod-driven signals. The other AII amacrine cells received contacts from only one of these two RB cells. An AII amacrine cell contacted nine to 12 RB cells; however, the number of contacts per RB–AII connection varied greatly (from one to more than 30). Approximately 60% of the contacts at most RB axons were directed to only one preferred AII amacrine cell. Thus, the signals derived from one rod were focused on a limited number of AII amacrine cells. Subsequently, they were coupled with each other via AII–AII gap junctions.

Bifurcation of a single-photon signal at most rod spherules

At a first stage, the examination of every rod spherule and its contacts with RB cells revealed a map of rod–RB connections. We found that most (94%) rods diverged to two RB cells and that a small fraction (6%) diverged to a single RB cell. Thus, the average divergence was 1.94. Conversely, the average convergence of rods to RB cells was 25 (Fig. 3). These figures are similar to those obtained for cats (Freed et al., 1987). This bifurcation of the output from a rod may result in two replicates of its signal (Fig. 4A). Because these replicates are driven by a single photon, they will be strongly correlated, which we hypothesize is crucial for the circuit's function.

We also found two unusual types of synaptic architecture, in which an RB cell received a rod signal from two active zones: a Y-shaped invaginating dendrite and a pair of invaginating dendrites extending from an RB cell. Although the function of these unusual connections is unknown, a comparison of the transfer characteristics of the rod–RB connection between one active zone and two active zones may determine their significance.

Dominance in RB–AII connections and unification of common rod-driven signals

At the next interface between RB and AII amacrine cells, on average 11 RB cells converge to one AII amacrine cell. All 55 possible pairs among the 11 RB cells were not necessarily connected to any common rods. Two RB cells were able to share a common rod in the area where their dendritic fields overlapped. Under the scotopic condition that only one of the hundreds of rods can absorb a single photon, among the 11 RB cells, only two RB cells that were connected to that same rod may work in signal transmission. Conversely, the divergence of one RB cell to 4.7 AII amacrine cells means that one RB cell simultaneously supplies output to four or five AII amacrine cells. One RB cell provided an uneven number of contacts to those AII amacrine cells. The largest number ranged from 29 to 41, which represented 61% of the total of RB contacts, on average (Table 2). Thus, many more contacts were allocated to this dominant connection from the RB cell to its preferred AII amacrine cell than to several other connections that shared the remaining contacts. Some RB cells, however, had no such single dominant connection; rather, they exhibited two equally weighted connections (e.g., RB14: 25 contacts with AII 2 and 24 contacts with AII 3). The convergence to divergence ratio (2.3) indicates that approximately two RB cells are in close proximity to one AII amacrine cell. It is highly likely that one AII amacrine cell is equipped with two dominant connections with these two nearest RB cells. When these two RB cells receive signals derived from the same rod, those common signals will be reunited at

this AII amacrine cell. Such a double dominant reunion occasionally occurred depending on the connectivity between individual rods and these two RB cells (Fig. 6B). In another case, two dominant connections conveying the common rod-driven signals were directed to two adjacent AII amacrine cells (Fig. 9). Because each of the two RB cells distributed the same signals to its four or five neighboring AII amacrine cells, each of the two AII amacrine cells frequently received the common rod-driven signals from one RB cell via dominant and the other via nondominant connections. In yet another case, one AII amacrine cell had no pathway to receive the common rod-driven signals from both RB cells; rather, it received from only one of them, because the other RB cell was at a distance. The two separate streams of the common rod-driven signals departing from two RB cells may be unified by electrical coupling via AII–AII gap junctions. All the AII amacrine cells may be coupled with one another in their syncytial network. The manner in which the balance between these one-step and two-step unifications of the common rod-driven signals affects the total performance remains to be elucidated.

Comparison between mouse and rabbit retinas

The only data set available for comparison in terms of dominant connections was presented by Strettoi et al. (1992), who reconstructed one whole AII amacrine cell in the rabbit retina. One particular RB cell had a total of 27 output ribbon contacts and supplied the largest number of contacts (15 contacts; 56% of the total outputs) to its preferred AII amacrine cell. This AII amacrine cell had a total of 47 input contacts with nine RB cells but received 32% of the total input only via this dominant RB–AII connection. It appears clear that preferential pathways are furnished in the RB–AII interconnection in both mouse and rabbit retinas. The specifications of this system, however, differ between them. The total number of RB output contacts was 53 in the mouse compared with only 27 in the rabbit retina; moreover, the total number of AII input contacts was 125 in the former compared with 47 in the latter (i.e., twice or more in the mouse than in the rabbit retina). For each cell receiving such a number of input contacts, one AII amacrine cell is equipped with two dominant connections in the mouse but with only one in the rabbit retina. The sum of the first and second largest numbers of AII input contacts provided by two dominant RB cells was 66 (53%) in the mouse (Table 2), whereas that provided by one dominant and one nondominant RB cells was 22 (47%) in the rabbit retina. It is noteworthy that approximately half of the AII input contacts are provided by only two RB cells in both species.

Implications for signal processing

The functional significance of this circuit may reside in its effect on synaptic noise, which would be incessantly generated at every release site throughout the RB–AII interface. In this intercellular transmission, the signal components are correlated because of their derivation from a common rod; however, noise components are uncorrelated because of their inherent randomness among a number of different release sites. The signal averaging performed in a relatively narrow space constant of AII–AII electrical coupling will remove uncorrelated noise components of the common rod-driven signals, allowing a great improvement in the S/N ratio of the correlated components (Smith and Vardi, 1995). One of the significant aspects of focusing action of this circuit is the avoidance of gathering any unnecessary noise from a wide surrounding area. The other is the intensification of signal amplitude in a narrow space by preventing signal dissipation. The S/N ratio (mean/standard deviation) in a circuit that sums currents converging from multiple synaptic contacts will be improved as the number of those contacts increases. Both functions may contribute to the representation of the original rod signal reliably. However, such amplification with focal accumulation may encounter a serious problem of response saturation. There is ample experimental evidence for the existence of high amplification and also mechanisms that circumvent the ceiling effect, as discussed below.

High-gain amplification and local-gain control

Dunn, Rieke, and colleagues (Dunn et al., 2006; Dunn and Rieke, 2008) have shown that a flash producing one Rh*/rod bipolar (0.25–0.5 Rh*effective/rod bipolar) produces a barely discernible response in a rod bipolar cell (~3% of maximal response) but produces nearly half-maximal response in an AII amacrine cell. Pang et al. (2007) also have found that the highest gain of the RB–AII synapse is approximately fivefold near the dark membrane potential. If a signal with such a high gain in the AII amacrine cell is evoked by only a few ribbon contacts, the resulting response would have a low S/N ratio. However, as indicated in this study, when the input is transmitted via dozens of separate ribbon contacts, the independent synaptic noise will be cancelled, yielding a more reliable response with high gain. This suggests that the large number of ribbon contacts observed at the dominant connection between

individual RB cells and AII amacrine cells (Figs. 4–6, Table 2) contributes to the mechanism of high-gain amplification.

As indicated by Dunn and Rieke (2008), the gain of the synaptic inputs to AII amacrine cells must be controlled to prevent saturation of these cells. Their results indicate that the gain of each RB–AII amacrine synapse is controlled primarily locally, without much influence from nearby RB cells, and is likely caused by changes in transmitter release (Singer and Diamond, 2006). The focal transmission by dominant connections from RB cells to their preferred AII amacrine cells (Figs. 5,6, Table 2) is necessarily localized. Because of the narrowness of that space, the response may easily saturate the dynamic range, but this effect is confined to that space. Our finding of dominant connections represents a structural basis for the requirement of local adaptation.

Initial phase of the AII amacrine response

Spike-like potentials have been recorded from AII amacrine cells in slice preparations from rats (Boos et al., 1993) and mice (Tamalu and Watanabe, 2007; Tian et al., 2010). The Na^+ channel subunit $Na_v1.1$ has been immunolabeled by using in situ hybridization in AII amacrine cells (Kaneko and Watanabe, 2007) and then localized to its AIS-like processes by ChR2-GFP-Na_vII–III expression and patch-clamp recordings (Wu et al., 2011). Our ultrastructural observations have substantiated the morphology of the AIS-like processes (Fig. 8). A study of responses in the AII amacrine cell by Tian et al. (2010) has revealed that the Na^+ channel-dependent acceleration, but not amplification, is reflected in the dynamics of AII synaptic output to retinal ganglion cells. The authors suggested that the initial rising phase of the AII response, rather than its peak amplitude, carries the salient information regarding scotopic rod signals. In this context, our results suggest that the slope of the rising phase in the AII amacrine cell, as a nonsaturating signal, is enhanced by the large number of synaptic inputs from each dominant RB cell. Because this initial phase response rapidly occurs with a relatively short period of temporal summation, spatial summation within one AII amacrine cell or a few electrically coupled AII amacrine cells may be of critical importance for the reliability of this rod signal.

CONCLUSIONS

The rod–RB–AII microcircuits of the mouse retina have three characteristic architectures: 1) a system of bifurcation at the rod output and reunion at the AII input, 2) focusing of each RB output on a single preferred AII amacrine cell via the dominant connection, and 3) spatial unification of neighboring AII amacrine cells by electrical coupling. By means of duplication (~2) and multiplication (~50), this microcircuit architecture will make approximately 100 replicates of a rod single-photon signal at RB axon ribbon synaptic contacts. When transmitted through noisy synaptic release at the RB active zones, most of those common rod-driven signals will be focused on and accumulated in a few AII amacrine cells, to represent the original signal reliably without gathering unnecessary noise from a wide surrounding area. Thus, based on our quantitative 3D reconstructions, the high amplification, local adaptation, and regenerative acceleration of the scotopic signal responses found in physiological recordings of AII amacrine cells appear to be deeply rooted in the structural connectivity of the circuit.

ACKNOWLEDGMENTS

We thank Dr. Robert G. Smith at the University of Pennsylvania for comments on the manuscript and Ms. Satoko Inoue for providing technical assistance.

CONFLICT OF INTEREST STATEMENT

The authors have no conflict of interest.

ROLE OF AUTHORS

All authors had full access to all the data in the study and take full responsibility for the integrity of the data and the accuracy of data analysis. Study concept and design: YT. Acquisition, analysis, and interpretation of data: YT, NO. Drafting of the manuscript: YT.

LITERATURE CITED

Barlow HB, Levick WR, Yoon M. 1971. Responses to single quanta of light in retinal ganglion cells of the cat. Vis Res Suppl 3:87–101.

Baylor DA, Lamb TD, Yau KW. 1979. Responses of retinal rods to single photons. J Physiol 288:613–634.

Baylor DA, Nunn BJ, Schnapf JL. 1984. The photocurrent, noise and spectral sensitivity of rods of the monkey *Macaca fascicularis*. J Physiol 357:575–607.

Bloomfield SA. 2001. Plasticity of AII amacrine cell circuitry in the mammalian retina. Prog Brain Res 131:185–200.

Bloomfield SA, Xin D. 2000. Surround inhibition of mammalian AII amacrine cells is generated in the proximal retina. J Physiol 523:771–783.

Bloomfield SA, Xin D, Osborne T. 1997. Light-induced modulation of coupling between AII amacrine cells in the rabbit retina. Vis Neurosci 14:565–576.

Boos R, Schneider H, Wassle H. 1993. Voltage- and transmitter-gated currents of all-amacrine cells in a slice preparation of the rat retina. J Neurosci 13:2874–2888.

Boycott BB, Kolb H. 1973. The connections between bipolar cells and photoreceptors in the retina of the domestic cat. J Comp Neurol 148:91–114.

Dunn FA, Rieke F. 2008. Single-photon absorptions evoke synaptic depression in the retina to extend the operational range of rod vision. Neuron 57:894–904.

Dunn FA, Doan T, Sampath AP, Rieke F. 2006. Controlling the gain of rod-mediated signals in the mammalian retina. J Neurosci 26:3959–3970.

Field GD, Rieke F. 2002. Nonlinear signal transfer from mouse rods to bipolar cells and implications for visual sensitivity. Neuron 34:773–785.

Freed MA, Smith RG, Sterling P. 1987. Rod bipolar array in the cat retina: pattern of input from rods and GABA-accumulating amacrine cells. J Comp Neurol 266:445–455.

Ishii M, Morigiwa K, Takao M, Nakanishi S, Fukuda Y, Mimura O, Tsukamoto Y. 2009. Ectopic synaptic ribbons in dendrites of mouse retinal On- and Off-bipolar cells. Cell Tissue Res 338:355–375.

Kaneko Y, Watanabe S. 2007. Expression of $Na_v1.1$ in rat retinal AII amacrine cells. Neurosci Lett 424:83–88.

Linberg K, Cuenca N, Ahnelt P, Fisher S, Kolb H. 2001. Comparative anatomy of major retinal pathways in the eyes of nocturnal and diurnal mammals. Prog Brain Res 131: 27–52.

Mastronarde DN. 1983. Correlated firing of cat retinal ganglion cells. II. Responses of X- and Y-cells to single quantal events. J Neurophysiol 49:325–349.

Oesch NW, Diamond JS. 2011. Ribbon synapses compute temporal contrast and encode luminance in retinal rod bipolar cells. Nat Neurosci 14:1555–1561.

Palay SL, Sotelo C, Peters A, Orkand PM. 1968. The axon hillock and the initial segment. J Cell Biol 38:193–201.

Pang JJ, Gao F, Wu SM. 2004. Light-evoked current responses in rod bipolar cells, cone depolarizing bipolar cells and AII amacrine cells in dark-adapted mouse retina. J Physiol 558:897–912.

Pang JJ, bd-El-Barr MM, Gao F, Bramblett DE, Paul DL, Wu SM. 2007. Relative contributions of rod and cone bipolar cell inputs to AII amacrine cell light responses in the mouse retina. J Physiol 580:397–410.

Pang JJ, Gao F, Wu SM. 2012. Physiological characterization and functional heterogeneity of narrow-field mammalian amacrine cells. J Physiol 590:223–234.

Peters A, Proskauer CC, Kaiserman-Abramof IR. 1968. The small pyramidal neuron of the rat cerebral cortex. The axon hillock and initial segment. J Cell Biol 39:604–619.

Rieke F. 2008. Seeing in the dark: retinal processing and absolute visual threshold. In: Masland RH, Albright TD, editors. The senses, vol.1. Vision I. New York: Academic Press/Elsevier. p 393–412.

Sampath AP, Rieke F. 2004. Selective transmission of single photon responses by saturation at the rod-to-rod bipolar synapse. Neuron 41:431–443.

Singer JH, Diamond JS. 2006. Vesicle depletion and synaptic depression at a mammalian ribbon synapse. J Neurophysiol 95:3191–3198.

Singer JH, Lassova L, Vardi N, Diamond JS. 2004. Coordinated multivesicular release at a mammalian ribbon synapse. Nat Neurosci 7:826–833.

Smith RG, Vardi N. 1995. Simulation of the AII amacrine cell of mammalian retina: functional consequences of electrical coupling and regenerative membrane properties. Vis Neurosci 12:851–860.

Sterling P, Freed MA, Smith RG. 1988. Architecture of rod and cone circuits to the on-beta ganglion cell. J Neurosci 8:623–642.

Strettoi E, Raviola E, Dacheux RF. 1992. Synaptic connections of the narrow-field, bistratified rod amacrine cell (AII) in the rabbit retina. J Comp Neurol 325:152–168.

Tamalu F, Watanabe S. 2007. Glutamatergic input is coded by spike frequency at the soma and proximal dendrite of AII amacrine cells in the mouse retina. Eur J Neurosci 25: 3243–3252.

Tian M, Jarsky T, Murphy GJ, Rieke F, Singer JH. 2010. Voltage-gated Na channels in AII amacrine cells accelerate scotopic light responses mediated by the rod bipolar cell pathway. J Neurosci 30:4650–4659.

Tsukamoto Y, Morigiwa K, Ueda M, Sterling P. 2001. Microcircuits for night vision in mouse retina. J Neurosci 21: 8616–8623.

Tsukamoto Y, Morigiwa K, Ishii M, Takao M, Iwatsuki K, Nakanishi S, Fukuda Y. 2007. A novel connection between rods and On cone bipolar cells revealed by ectopic metabotropic glutamate receptor 7 (mGluR7) in mGluR6-deficient mouse retinas. J Neurosci 27:6261–6267.

van Rossum MC, Smith RG. 1998. Noise removal at the rod synapse of mammalian retina. Vis Neurosci 15:809–821.

Vardi N, Smith RG. 1996. The AII amacrine network: coupling can increase correlated activity. Vis Res 36:3743–3757.

Veruki ML, Hartveit E. 2002. AII (rod) amacrine cells form a network of electrically coupled interneurons in the mammalian retina. Neuron 33:935–946.

Wu C, Ivanova E, Cui J, Lu Q, Pan ZH. 2011. Action potential generation at an axon initial segment-like process in the axonless retinal AII amacrine cell. J Neurosci 31:14654–14659.